# Frequency-Resolved Optical Gating of Isolated Attosecond Pulses in the Extreme Ultraviolet

A. Kosuge, T. Sekikawa, X. Zhou, T. Kanai, S. Adachi, and S. Watanabe

*Institute for Solid State Physics, University of Tokyo, 5-1-5 Kashiwanoha, Kashiwa 277-8581, Japan*

(Received 20 June 2006; published 27 December 2006)

The pulse shape and phase of isolated attosecond extreme ultraviolet (XUV) pulses with a duration of 860 asec have been determined simultaneously by using frequency-resolved optical gating based on two-photon above-threshold ionization with 28-eV photons in He. From the detailed characterization, we succeeded in shaping isolated XUV pulses on an attosecond time scale by precise dispersion control with Ar gas density or by changing the driving pulse width. These results offer a novel way to excite and observe an electron motion in atoms and molecules.

DOI: 10.1103/PhysRevLett.97.263901 PACS numbers: 42.65.Re, 32.80.Fb, 42.65.Ky

Generation of attosecond pulses by high-order harmonics has drawn much attention in taking a snap shot of electron motion on an attosecond time scale. Various efforts have been made to generate isolated attosecond pulses [1–3] and pulse trains [4–7]. However, there has not been the full characterization of attosecond pulses where the pulse shape and phase should be determined uniquely. In the visible wavelength range, the pulse shape and phase of few-cycle pulses have been successfully characterized by frequency-resolved optical gating (FROG) [8] and spectral phase interferometry for direct electric-field reconstruction (SPIDER) [9]. However, in the spectral region of high-order harmonics, the applications of these techniques have been limited to longer pulses (not in the attosecond domain) of lower-order harmonics [10–12]. Some variants and alternatives [1–7] for FROG and SPIDER have been attempted to characterize attosecond pulses, but it has been impossible to determine the pulse shape and phase uniquely, i.e., without any assumption and simulation assist. In the FROG measurement, the pulse shape and phase are reconstructed from the time-frequency map of the spectra induced by nonlinear process versus the time delay between the relevant pulse and reference pulse. However, for the application of FROG to high-order harmonics, there are two difficulties: low harmonic intensity and no available nonlinear crystals. Usually two-photon ionization is used as a nonlinear process in the high-order harmonics. Two-color two-photon ionization with the harmonics and their intense fundamental radiation relaxes the difficulty somewhat. However, the measurable pulse duration is limited by the optical cycle of the fundamental pulse, which is 2.7 fs at 800 nm. Therefore, single-color two-photon ionization should be used to characterize an attosecond pulse, where the attosecond pulse itself works as a reference pulse [13,14]. Here we demonstrate the FROG measurement based on single-color two-photon above-threshold ionization (ATI) [13] where the photon energy is above the ionization potential of He. This was realized by the intense harmonics generated with a short wavelength (400 nm) laser in the nonadiabatic regime where ionization progresses rapidly [3,15], along with improved electron counting. The precise characterization of attosecond pulses enables insight into the generation process and the control of the pulse shape and phase.

The experimental setup is similar to Ref. [3]. A 1-kHz, terawatt-class Ti:sapphire laser was used to generate the second harmonic by a broadband frequency doubling scheme [16–18]. Broadband frequency doubling enabled us to shorten the pulse duration with high efficiency. This 400-nm (3.1-eV) source can produce sub-10-fs, sub-TW pulses. Two optically delayed replicas of the blue pulses were focused to a peak intensity of $6 \times 10^{14}$ W/cm$^2$ by a 50-cm-focal-length mirror to generate high-order harmonics in Ar supplied from a pulse gas jet. At this intensity, nearly complete ionization occurs because the intensity of a 98%-ionization level is $4.8 \times 10^{14}$ W/cm$^2$ in Ar at 15 fs [19,20]. The pulse gas jet was placed 4 mm after the focus to prevent the spatial overlap of two high harmonic beams. If the two beams are overlapped, the first pulse ionizes Ar and no harmonics are generated at the second pulse. After passing through an Al filter which eliminates the fundamental and lower-order harmonic pulses, the ninth harmonic was selected and focused in He by a Sc/Si multilayer mirror with a focal length of 5 cm. The photoelectrons ejected by two-photon ATI were collected and energy resolved by a magnetic bottle time-of-flight (TOF) photoelectron spectrometer with a counting system. The pulse energy of the ninth harmonic was approximately several nJ on target. We increased the ATI signal by 2–3 orders of magnitude and improved the resolution of a TOF photoelectron analyzer compared with the previous work [3]. The Ar gas density was increased by a factor of 2–3 by stabilizing the gas jet with water cooling [21]. The driving intensity was concentrated in the main pulse by suppressing the pedestal. As a result, the harmonic intensity was increased by 1 order of magnitude mainly because it is proportional to roughly the square of gas density, giving a 2 orders of magnitude higher two-photon signal. The replacement of a counter to a low-noise one enabled the use of an amplifier ( $\times$ 10). Then the total enhancement

 

of two-photon signals was 3 orders of magnitude at best.

Figure 1(a) shows the energy diagram of the two-photon ATI in He. Figure 1(b) shows a typical two-photon spectrum by the ninth harmonic. The horizontal axis corresponds to the energy of ejected electrons plus the ionization potential of He. We used a 8.3-fs driving pulse at a 7.5-torr Ar pressure. The harmonic spectrum was broad enough to ensure 700 asec at the transform limit. However, the longer wavelength part of the two-photon spectrum was hindered by a one-photon noise spectrum. We found spectral overlap was eliminated by cutting a driving spectrum above 413 nm. This was done by inserting a knife edge in the part of the regenerative amplifier where the spectrum is dispersed spatially [18]. The change of the pulse width was also done in the same way. This method is superior to cutting the output spectrum because full energy extraction is possible. As a result, the time width of the driving pulse was 15 fs, which is nearly transform limited, with an energy of 1.8 mJ. The pulse shape and phase of the driving pulse were determined by the self-diffraction FROG [16]. The Ar gas density was 7.2 torr. The spectral resolution was approximately 200 meV. The two-photon spectrum dominates clearly over the background noise and the one-photon

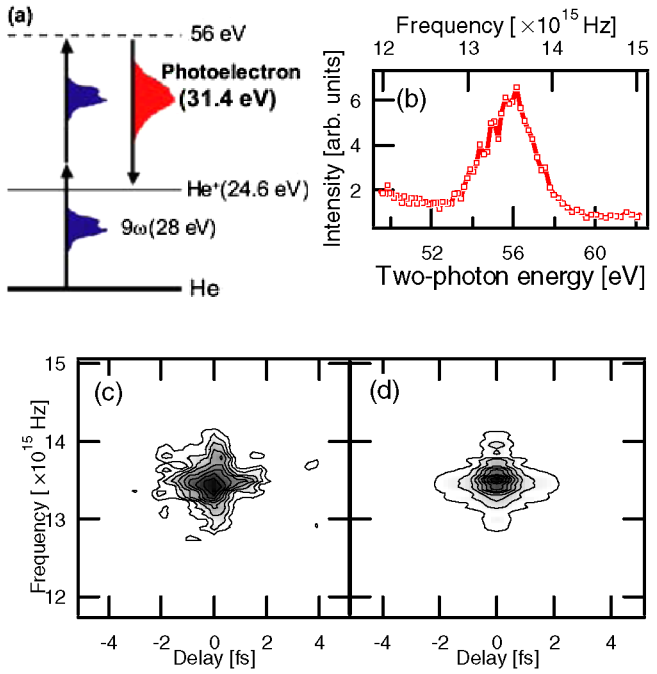


FIG. 1 (color online). (a) Energy diagram of two-photon above-threshold ionization in He. (b) Electron spectrum by two-photon above-threshold ionization. The horizontal axis is the electron energy plus the ionization potential of He. (c) Measured time-frequency map of the spectrum versus time delay between two replicas of ninth harmonic pulses. The signal intensity is expressed by contours with 10 steps from the top to the ground. (d) Time-frequency map retrieved from (c) by the iterative Fourier-transform algorithm with generalized projection. The root-mean-square error between (c) and (d) is 2.6%.

spectra. As the final states of two-photon absorption, doubly excited states, such as $2s^2\,{}^1S$ and $2p^2\,{}^1D$, should be taken into account. The $2p^2\,{}^1D$ state (60 eV) is obviously off resonant as shown in Fig. 1(b). However, the observed two-photon spectrum marginally covers only $2s^2\,{}^1S$ at 58 eV [22]. Although we were so careful to observed the potential resonance peak due to the autoionization from $2s^2\,{}^1S$, no peaks were observed throughout the experiment, which should be attributable to small spectrum density of the high harmonic pulse above 29 eV. We think some scattering in the calculation of the two-photon ionization cross section [22] needs to be fixed for further argument. This clear and well-resolved spectrum without resonance structures enabled us to use the FROG measurement. ATI-FROG traces were obtained by measuring the two-photon spectrum at each optical delay. The corresponding two-photon spectrogram is expressed as [8]

$$I_{\mathrm{FROG}}(\omega, \tau) = \left| \int_{-\infty}^{\infty} E(t)E(t-\tau)\exp(-i\omega t)dt \right|^2, \quad (1)$$

where $\tau$ is the optical delay, $E(t)$ is the time-dependent electric field, and $\omega$ is the optical frequency.

Figure 1(c) depicts the measured ATI-FROG trace corresponding to $I_{\mathrm{FROG}}(\omega, \tau)$. The vertical and horizontal axes correspond to the frequency and the optical delay time, respectively. The time-independent background by two-photon ATI and the mean background of random noise were subtracted beforehand, and super-Gaussian corner suppression and low pass filters were applied for optimal preparation of an ATI-FROG trace [23]. The pulse was retrieved by the use of the iterative Fourier-transform algorithm with generalized projection [24]. This procedure is mathematically verified to give a unique solution of $E(t)$, i.e., the pulse shape and phase. Figure 1(d) is the retrieved FROG trace. The root-mean-square error between the measured and retrieved traces was 2.6%. The trace shows a single isolated pulse. The corresponding pulse shape and phase are shown in Fig. 2(b).

Figure 2 shows the retrieved temporal profile and phase of the ninth harmonic pulse for various conditions of Ar gas density and driving pulse width. The pulse shape is expressed by the intensity corresponding to the square of the envelope. The black dashed curves show the transform-limited pulses calculated from the spectra of the ninth harmonic. Figures 2(a)–2(c) show the dependence of the pulse shape and phase on Ar gas density with a fixed pulse width (15 fs) of the driving laser. Figures 2(a)–2(c) correspond to the gas pressure of 5.7, 7.2, and 9.4 torr, respectively. The Ar gas density was determined by the comparison between the side fluorescence from the pulse gas jet in the vacuum and that of a static gas cell. The reabsorption of the fluorescence in the static cell was not considered for the calibration because the short wavelength below 400 nm was eliminated by the sensitivity of a CCD camera [25,26]. Then the gas density corresponds to the pressure at room temperature (293 K). Figures 2(b) and

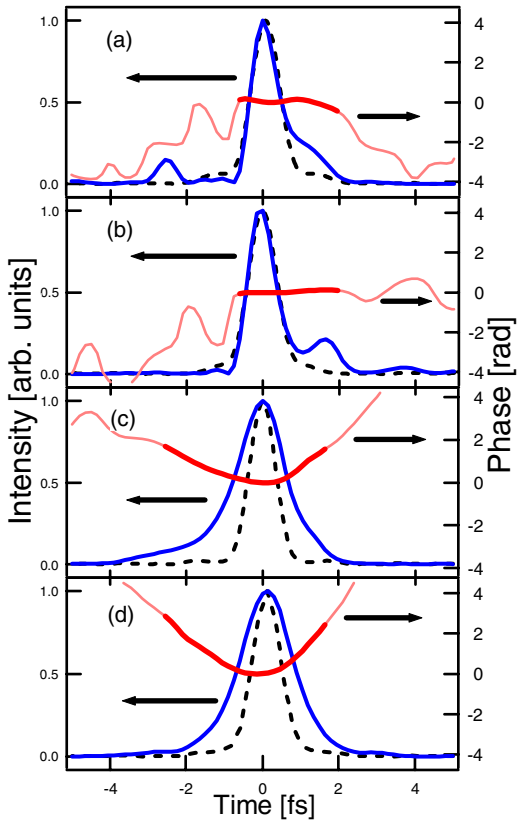


FIG. 2 (color online). Retrieved pulse shapes and phases. The dashed curves show the transform-limited pulse shapes. Thick solid curves in the phase correspond to the entire pulse and are used to determine the quadratic chirp coefficients. (a), (b), and (c) correspond to Ar gas densities of 5.7, 7.2, and 9.4 torr, respectively, with a fixed driving pulse width of 15 fs. (d) corresponds to a driving pulse width of 19 fs with an Ar density of 7.2 torr. (a), (b), and (c) show the dependence of the pulse shape and phase on Ar gas density. (b) and (d) show the dependence on driving pulse width.

2(d) show the dependence of the pulse shape and phase on pulse width of the driving laser with a fixed Ar gas density of 7.2 torr. Figures 2(b) and 2(d) correspond to the driving pulse widths of 15 and 19 fs, respectively. The drastic changes in the pulse shape and phase were observed among these 4 panels of Fig. 2. It should be noted that the pulse shape and phase can be controlled actively by adjusting parameters such as gas density and driving pulse width. The time direction ambiguity arising from the two-photon process was removed in the following ways. In the case of nearly transform-limited pulses such as Figs. 2(a) and 2(b), the pulse tail was directed to the back, because the present scheme of attosecond generation brings about the pulse tail [3]. In the case of chirped pulses such as Figs. 2(c) and 2(d), the time direction was determined by the fact that the chirp should be positive, because the high energy tail by self-phase modulation (SPM) will appear in the latter part of the driving pulse in the present scheme, as mentioned in detail below. In the present scheme, the temporal phase is determined mainly by the dynamic balance among the dispersions caused by the atomic dipole, free electrons, and Ar gas in the case of the transform-limited driving pulses. The simulation based on the Ammosov-Delone-Krainov theory [27] about the ionization and the zero-range potential model [28] about atomic dipole moment gives an almost flat phase in appropriate conditions such as Figs. 2(a) and 2(b) [11].

Figure 3(a) shows the Ar gas density dependence of the ninth harmonic spectra. As increasing Ar gas density, we observed a significant change of spectral shapes. At 3.5 torr or less, the spectrum reflects well the driving pulse and is what is expected from 9 times the photon energy of the driving pulse (within the dotted lines). However at a higher gas density, the spectral range was expanded, in particular, on the high energy side. There are some origins of spectral broadening due to SPM. The atomic dipole phase of harmonics induces a blueshift in the leading edge, but does not depend on gas density. The optical Kerr effect in the driving pulse gives a redshift in the leading edge and is quite small in the present condition. Free electrons cause a blueshift of the driving pulse, inducing a magnified blueshift in harmonics [29]. Therefore we concluded free electrons mainly contributed to the observed blueshift. Because the frequency sweep is proportional to the time derivative of electron density but not the total density, it is maximized

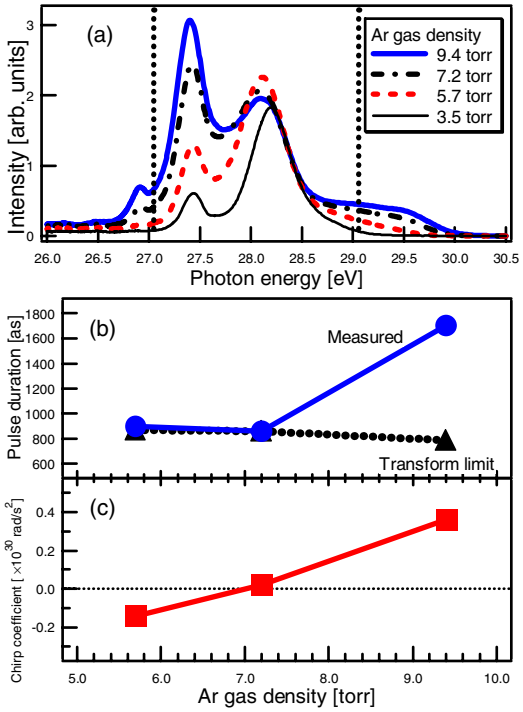


FIG. 3 (color online). (a) Harmonic spectra at Ar densities of 9.4 torr (thick solid carve), 7.2 torr (dot-dashed carve), 5.7 torr (dashed carve), and 3.5 torr (thin solid carve), respectively. The dotted lines show the spectral range corresponding to 9 times the spectral band of the driving pulse. (b) The dependence of measured (solid line) and transform-limited pulse durations (dotted line) on Ar gas density. (c) The quadratic chirp coefficients depending on Ar gas density.

during harmonic generation. The estimated blueshift is 1 eV at 10 torr, in good agreement with the experiment [3,10]. The peaks at 27.4 eV are almost proportional to the square of gas density, while the peaks at 28.1 eV do not change because the spectral component flows to the higher energy by the blueshift.

Figure 3(b) depicts the dependence of the pulse duration and the transform-limited pulse duration on Ar gas density. Figure 3(c) shows the dependence of the quadratic chirp coefficients on Ar gas density. The pulse durations and quadratic chirp coefficients were taken from Figs. 2(a)–2(c). The quadratic chirp coefficients were obtained by fitting the parabolic functions to the thick curves in Figs. 2(a)–2(c), which cover the entire pulses. The transform-limited pulse durations were calculated from Fig. 3(a). The FROG trace was not taken at 3.5 torr because of insufficient two-photon signal. The significant features of Figs. 3(a)–3(c) are as follows. First, spectral broadening was not observed at 3.5 torr, which is still a little higher than that of Ref. [3]. The transform-limited pulse duration of 1.3 fs is quite consistent with Ref. [3]. Second, the bandwidth ensuring the attosecond pulses comes from the spectral broadening in addition to 9 times the bandwidth of the driving pulse. Third, there is an optimum gas density which gives the dynamic balance among various dispersions due to the atomic dipole, free electrons, and optical Kerr effect, resulting in the nearly transform-limited 860-asec pulse at 7.2 torr [3,10]. The quadratic phase coefficient is almost proportional to Ar gas pressure and is minimized at 7.2 torr. At a higher gas density of 9.4 torr, a significant chirp was observed and the pulse width was broadened to 1.7 fs, which is approximately twice the transform limit, as shown in Figs. 3(b) and 3(c). At a lower gas density of 5.7 torr, a chirp is negative but relatively small, and a nearly transform-limited pulse (900 asec) was obtained. The measured quadratic coefficients of the phase are $-1.4 \times 10^{29}$ rad/s$^2$ at 5.7 torr, $0.2 \times 10^{29}$ rad/s$^2$ at 7.2 torr, and $3.6 \times 10^{29}$ rad/s$^2$ at 9.4 torr, respectively.

The pulse shaping by changing the driving pulse width shows similar behavior as shown in Figs. 2(b) and 2(d). The transform-limited pulse durations derived from the spectra are almost identical between two pulse widths (15 and 19 fs). This is because SPM in Ar dominates the spectrum. However, the measured pulse widths show a drastic change, resulting in 860 asec at 15 and 1.7 fs at 19 fs. The corresponding quadratic chirp coefficients were $0.2 \times 10^{29}$ rad/s$^2$ at 15 fs, $6.1 \times 10^{29}$ rad/s$^2$ at 19 fs, respectively. With the spectral broadening due to SPM over 9 times the bandwidth of a driving pulse, the phase was distorted, resulting in the pulse broadening. This is the same as the gas density dependence.

In conclusion, we have determined the shape and phase of isolated attosecond extreme ultraviolet (XUV) pulses simultaneously by using FROG based on two-photon ATI with 28-eV photons in He. The measured shortest pulse duration was 860 asec with a flat phase. From the detailed characterization, we have demonstrated the shaping of XUV pulses on an attosecond time scale by changing either the Ar gas density or the driving pulse width. The FROG measurement can be scalable to even sub-100-asec pulses. It is possible to extend this technique to the harmonic less than the first excited state of He+ (65 eV) [30], of which two-photon ATI cross section is also in the order of $10^{-52}$ cm$^4$ s. The technical issues such as the improvement of harmonic efficiency and electron counting should be solved to apply FROG to higher orders, although the cross section above $He^{2+}$ (79 eV) is not investigated theoretically. The scheme of nonadiabatic attosecond generation can be extend to sub-100-asec regime with higher-order harmonics by using a sub-TW, carrier-envelope phase-stabilized driving source with a pulse width around 5 fs.


[1] M. Hentschel *et al.*, Nature (London) **414**, 509 (2001).
[2] R. Kienberger *et al.*, Nature (London) **427**, 817 (2004).
[3] T. Sekikawa *et al.*, Nature (London) **432**, 605 (2004).
[4] P. M. Paul *et al.*, Science **292**, 1689 (2001).
[5] P. Tzallas *et al.*, Nature (London) **426**, 267 (2003).
[6] Y. Nabekawa *et al.*, Phys. Rev. Lett. **96**, 083901 (2006).
[7] K. Varju *et al.*, Phys. Rev. Lett. **95**, 243901 (2005).
[8] R. Trebino *et al.*, Rev. Sci. Instrum. **68**, 3277 (1997).
[9] C. Iaconis and I. A. Walmsley, Opt. Lett. **23**, 792 (1998).
[10] T. Sekikawa *et al.*, Phys. Rev. Lett. **88**, 193902 (2002).
[11] T. Sekikawa, T. Kanai, and S. Watanabe, Phys. Rev. Lett. **91**, 103902 (2003).
[12] Y. Mairesse *et al.*, Phys. Rev. Lett. **94**, 173903 (2005).
[13] N. Miyamoto *et al.*, Phys. Rev. Lett. **93**, 083903 (2004).
[14] Y. Kobayashi *et al.*, Opt. Lett. **23**, 64 (1998).
[15] I. P. Christov, M. M. Murnane, and H. C. Kapteyn, Phys. Rev. Lett. **78**, 1251 (1997).
[16] T. Kanai *et al.*, Opt. Lett. **28**, 1484 (2003).
[17] T. Kanai *et al.*, Opt. Lett. **29**, 2929 (2004).
[18] Y. Nabekawa *et al.*, Opt. Lett. **23**, 1384 (1998).
[19] B. Chang, P. R. Bolton, and D. N. Fittinghoff, Phys. Rev. A **47**, 4193 (1993).
[20] Z. Chang *et al.*, Phys. Rev. Lett. **79**, 2967 (1997).
[21] A. Flettner *et al.*, Appl. Phys. B **73**, 129 (2001).
[22] L. A. A. Nikolopoulos and P. Lambropoulos, J. Phys. B **34**, 545 (2001).
[23] D. N. Fittinghoff, J. Opt. Soc. Am. B **12**, 1955 (1995).
[24] S. Linden, H. Giessen, and J Kuhl, Phys. Status Solidi B **206**, 119 (1998).
[25] T. Adachi, K. Kondo, and S. Watanabe, Appl. Phys. B **55**, 323 (1992).
[26] L. A. Lompré *et al.*, J. Appl. Phys. **63**, 1791 (1988).
[27] M. V. Ammosov, N. B. Delone, and V. P. Krainov, Sov. Phys. JETP **64**, 1191 (1986).
[28] W. Becker, S. Long, and J. K. McIver, Phys. Rev. A **50**, 1540 (1994).
[29] T. Sekikawa *et al.*, J. Opt. Soc. Am. B **15**, 1406 (1998).
[30] T. Nakajimaand and L. A. A. Nikolopoulos, Phys. Rev. A **66**, 041402 (2002).